23PFL-0599

Effect of split-injection strategies on engine performance and emissions under cold-start operation

Author, co-author (Do NOT enter this information. It will be pulled from participant tab in MyTechZone)
Affiliation (Do NOT enter this information. It will be pulled from participant tab in MyTechZone)

Abstract

The recently concluded partnership for advancing combustion engines (PACE) was a US Department of Energy consortium involving multiple national laboratories focused on addressing key efficiency and emission barriers in light-duty engines. Generation of detailed experimental data and modeling capabilities to understand and predict cold-start behavior was a major pillar in this program. Cold-start, as defined by the time between first engine crank and three-way catalyst light-off, is responsible for a large percentage of NOx, unburned hydrocarbon, and particulate matter emissions in light-duty engines. Minimizing emissions during cold-start is a trade-off between achieving faster three-way catalyst light-off, and engine out emissions during that period. In this study, engine performance, emissions, and catalyst warmup potential were monitored while the engine was operated using a single direct injection (baseline case) as well as a two-way-equal-split direct injection strategy. These injection strategies were analyzed at a range of cold-start-operation relevant retarded spark timings of up to 25 degrees after top dead center of firing (dATDCf). A stoichiometric 2-bar NIMEP steady-state condition was used for all cases to simulate cold-start operation. Significant improvement in engine stability was observed with the two-way-split injection strategy at the retarded spark timings allowing for up to 2.5x increase in exhaust heat rate when engine operation is stability constrained. Similar fuel-loss-to-oil trends with exhaust heat rate were observed for both single and two-way-split injection strategies. However, the two-way split injection was observed to produce higher NOx emissions per unit exhaust heat rate. A single data point run with three-way-split direct injection at a very retarded spark-timing of 30 dATDCf pointed to further improvements in engine stability and reduction in fuel-loss-to-oil as compared to single injection strategy. Engine stability decreased as spark timing was initially retarded with a single injection but was observed to plateau and stabilize beyond spark timing of 10 dATDCf. For the two-way-split-injection strategy, retarding the start of injection (SOI) timing of the second injection led to a decrease in engine stability as well as an increase in soot emissions.

Introduction

Cold-start operation, which is defined as the time between first-crank and three-way-catalyst light-off, is emerging as the dominant source of pollutant emissions such as NOx, unburned hydrocarbons (HC), particulate matter mass (PM) and particulate matter number (PN) especially with recent improvements in aftertreatment system performance under warm conditions [1 - 4]. Acknowledging this trend, improved understanding and prediction of cold start operation through generation of detailed experimental data as well as modeling capabilities was a major pillar of the US Department of Energy's partnership for advancing combustion engines (PACE) initiative [5]. Cold start operation in light-duty spark-ignited engines has been the focus of multiple experimental [6 - 22] and computational [23 - 28] studies in literature. These studies have elucidated the impact of many engine parameters such as spark timing [6, 11], start of injection timing [14, 22], and cam timing [6, 9].

However, very few research articles tackle performance and emissions of direct-injected spark-ignited (DISI) engines when operating under cold-start relevant boundary conditions with split-injection strategies. Li et al. [17] demonstrated the effect of differing dwell times between the two injections of a split-injection scheme through laser absorption and scattering measurements in a constant volume chamber. It was shown that split-injection with optimized dwell times removes the fuel piling at the edge of the spray that occurs with the single injection and therefore can help reduce penetration depth of the dense-liquid phase of the spray. Furthermore, changing the dwell between the two injections also substantially impacted fuel-vapor distribution. In a subsequent study [18], Li et al also showed through optical spray imaging that air entrained behind a single injection can create very lean zone behind the spray, while injecting the second-injection into this entrained air can lead to improved vaporization of the second injection and improve air-fuel-ratio distribution. In this study, engine experiments with advanced ignition timing (-24 dATDCf) showed soot and NOx benefits with a split injection strategy while engine COV was not impacted. The strategy also resulted in increased engine out HC when compared to the single injection case. However, it should be noted that this ignition timing is early in the cycle and is not relevant for cold start operation. Mittal et al [19] investigated the impact of split injections on fuel wall wetting with a non-fired single-cylinder optical engine fueled by E85 at a 50bar injection pressure and observed split injection to reduce wall-wetting by up to 50%. Cedrone et al. [20] reported on split injection performance under cold-start conditions in a 4-cylinder engine over a wide range of second injection timings. Results showed that retarding the start of injection (SOI) timing of the second injection led to a reduction in engine stability while the exhaust heat rate increased. Furthermore, hydrocarbon emissions were also observed to decrease with retarding second injection SOI timing. However, a limited spark timing retard was used for the second injection SOI sweep leading to a low exhaust heat rate of ~3-4 kW/L. Engine original equipment manufacturers (OEMs) have also previously published findings on use of split injection in DISI engines and for cold-start performance improvement [21, 22] but these lack crucial boundary condition data required for them to be suitable for calibration/validation of CFD models. Stiesch et al. [25] reported on CFD investigation of the impact of split injection in a DISI engine and demonstrated that the timing of the second injection can be tuned to

create a rich zone near the spark plug and thus stabilize combustion. Zheng et al. [26] in a CFD study of split injection under catalyst warmup conditions, showed that retarding timing of the second injection negatively impacted in-cylinder mixture quality. However, the simulations were performed with an advanced spark timing of -10 dATDCf.

Therefore, despite existence of prior work on split injections in DI engines, knowledge gaps exist on how such injection strategies could impact engine performance and emissions while operating under cold-start relevant retarded spark timing and late cycle combustion. The main aim of this study is to help fill this knowledge gap by understanding how split injection strategies impact cold-start operation at a range of exhaust heat rate values beyond what has previously been reported in literature for cold-start operation. This work provides data that encompass a wide range of operating conditions, necessary for validation and development of computational models as well as study of the stability and cyclic variability properties of these extreme operating conditions. The results shown try to elucidate the mechanisms of observed engine performance and emissions behavior, and narrow down conditions for further analysis with advanced diagnostic techniques, engine testing, and computational fluid dynamic simulations.

Experimental Setup

This study utilizes a single-cylinder version of a GM LNF 2.0L DISI engine, wherein 3 of the cylinders were disabled by grinding the cam lobes to the base circle as well as drilling holes in the pistons to prevent compression. The firing cylinder was run in a stock configuration, wherein compression ratio, combustion chamber geometry, fuel injector, cam lobe profiles and cam phasing capabilities remained intact. Furthermore, stock high-pressure gasoline fuel pump, fuel rail, and oil pump were also retained. Engine specifications are listed in Table 1. The engine features extensive instrumentation (Figure 1) including high-speed transducers for intake port (Kistler 4007D), in-cylinder (Kistler 6125c), and exhaust port (Kistler 4049B) pressure measurements as well as various thermocouples for temperature measurements. Fuel flow was measured using a Coriolis flow meter (Micromotion CMFS007M). A combination of an external standalone air-compressor and a mass flow controller (Alicat MCR) was utilized to feed desired air flow into the engine. Intake and exhaust surge tanks were utilized to dampen pressure pulsations. Exhaust gas concentrations were measured using standard gas analyzers (CAI 600/700 series), i.e., non-dispersive infrared analyzers for CO_2 and CO, a paramagnetic analyzer for O_2, a flame ionization detector for total hydrocarbons (THC), and a chemiluminescent detector for NO_x measurements. The exhaust gas emissions sampling port was located 225 mm away from the exhaust port outlet. Soot was measured using an AVL micro-soot sensor. Finally, an external chiller was utilized to maintain engine-out oil and coolant temperatures at 20 °C. The intake manifold gas temperature was not controlled in this study and was observed to be ~27 °C for all data points presented here. This same setup was also used for our previously published cold-start work [6].

To eliminate fuel composition uncertainty from chemical-kinetics modeling activities, the PACE consortium developed a 9-component surrogate fuel blend known as PACE20 [29]. The % weight fraction specification of PACE20 sub-components is tabulated in Table 2. This blend was designed to closely mimic the fuel properties such as boiling range and octane rating, as well as engine emissions parameters such as sooting propensity of a market-representative 87 AKI E10 fuel. The PACE20 fuel used in this study was blended by Gage Products and the measured fuel properties are listed in Table 3.

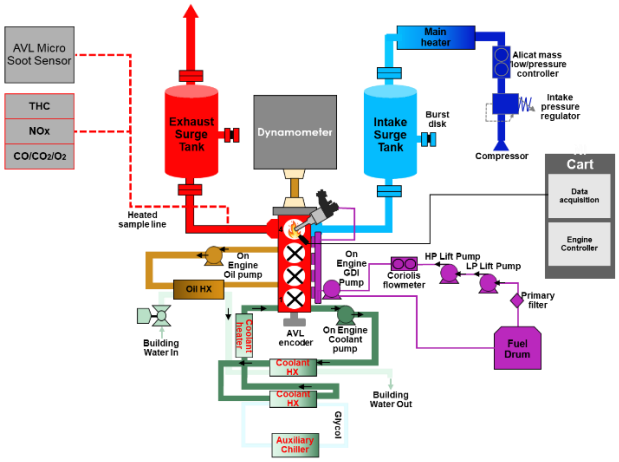

Figure 1: Single-cylinder engine system diagram

Table 1: Engine specifications

Bore	86 mm
Stroke	86 mm
Configuration	I-4 (single)
Compression Ratio	9.2:1
Ignition Coil Energy	80 mJ
Induction	Air compressor via air-mass flow controller
Fuel System	Side-mount gasoline direct injection

Table 2: PACE20 fuel composition

Sub-component Name	% Weight Fraction
Tetralin	3.85
1,2,4-trimethlybenzene	13.95
Toluene	10.74
iso-Octane	23.38
n-heptane	10.62
Ethanol	10.14
1-hexene	4.91
cyclo-pentane	10.66
n-pentane	11.75

Table 3: PACE20 fuel properties

Property [units]	Measurement Method	Value
Research Octane Number [-]	ASTM D2699	91.5
Motor Octane Number [-]	ASTM D2700	82.5
Octane Sensitivity [-]	RON – MON	9
Initial boiling point [°C]	ASTM D86	43.2
T10 [°C]	ASTM D86	56.8
T50 [°C]	ASTM D86	89.7
T90 [°C]	ASTM D86	165.9
Final boiling point [°C]	ASTM D86	189.9
Specific Gravity [-]	ASTM D4052	0.7465
Carbon [wt %]	ASTM D5291	82.9
Hydrogen [wt %]	ASTM D5291	13.6
Oxygen [wt %]	ASTM D4815	3.5
Lower Heating Value [MJ/kg]	ASTM D240mod	41.87

All measurements were taken during stoichiometric steady-state engine operation at 1300RPM and 2bar NIMEP. This speed/load condition was determined as a steady-state surrogate for the catalyst heating portion of the cold start operation research by the USDRIVE advanced combustion and emission control technical team (ACECTT) [30], which included input from many US light-duty-engine original equipment manufacturers (OEMs). The cold start protocol was not publicly released, but it was widely shared with DOE and the national labs participating in the PACE consortium to inform program research direction and goals. Air flow and fuel flow were optimized for each case to achieve engine-out stoichiometric operation at 2 bar NIMEP load. Air-fuel ratio was calculated from exhaust gas analyzer measurements using a LabVIEW version of the Engine Emissions & Uncertainty Analysis code developed by Dempsey and Ghandhi [31]. This exhaust lambda calculated from exhaust emissions measurements

was also used to control engine stoichiometry. Engine control was provided by a National Instruments Powertrain Controls Engine Control System (ECS) that is capable of next-cycle control action, with an integrated in-house Oak Ridge Combustion Analysis System (ORCAS) performing heat release and other combustion analysis calculations. The fuel injection pressure was set at 120 bar for all conditions. Both the intake and exhaust cams were fixed at the 'parked positions' (0 CAD phasing) where maximum negative valve overlap (NVO) is also achieved. This study did not employ any external exhaust gas recirculation.

Engine performance and emissions were compared for single and split direct injection strategies including single direct injection (1xDI) as a baseline as well as two-equal-way-split direction injection (2xDI) and three-equal-way-split direction injection (3xDI) strategies. Details of the three strategies are tabulated in Table 4. For the 1xDI strategy, the spark timing was swept from a relatively advanced timing of -10 degrees after top dead center of firing (dATDCf) to a very retarded cold-start relevant timing of 25 dATDCf in steps of 5 CAD. The 2xDI strategy repeated the spark timing sweep to a 25 dATDCf spark timing but could not be run at spark timings more advanced than 10 dATDCf. The fuel flow requirements at these advanced timings were low enough such that the injection duration fell below the capabilities of the injection system used in this study. Finally, due to time constraint, only one datapoint of the 3xDI injection was run and is included as an indicator of how higher split-count strategies could perform. This 3xDI point was run at a spark timing of 30 dATDCf which is more delayed than the spark timing sweeps of the 1xDI and 2xDI strategies. More data at 3xDI would be required to establish trends. As shown in Figure 2e, at 25 dATDCf spark timing, both 1xDI and 2xDI strategies required near non-throttled operation with the intake manifold pressure (IMP) of 0 kPa and -2kPa gauge, respectively, while the 30 dATDCf spark timing 3xDI data point required boosted operation (26.7 kPa gauge IMP). The 1xDI strategy injection as well as the first injection of 2xDI and 3xDI strategies were run with a fixed start-of-injection timing (SOI) of -270 dATDCf. For this study, the follow-on injections for the multi-injection strategies were close coupled to the initial injection, with the 2nd injection run at a SOI timing of -240 dATDCf, and the third injection of the 3xDI strategy run at a timing of -210 dATDCf. Furthermore, the SOI timing of the second injection of the 2xDI strategy was swept from -240 dATDCf to -200 dATDCf to assess the impact of a delayed second injection.

Table 4: Spark and injection timings for the three direct-injection strategies.

Direct Injection Strategy	Marker	Injection #	Spark Timing Range	SOI Range
			dATDCf	dATDCf
Single	1xDI	Injection 1	-10 to 25	fixed @ -270
Two-way split	2xDI	Injection 1	10 to 25	fixed @ -270
		Injection 2		-240 to -200
Three-way split	3xDI	Injection 1	30	-270
		Injection 2		-240
		Injection 3		-210

Results and Discussion

Effect of split injection strategies under cold-start operation at various spark timings

Cold-start engine operation was evaluated at spark timings ranging from -10 to 25 dATDCf for single direct injection strategy and from 10 to 25 dATDCf for the double injection strategy and trends in performance parameters are shown in Figure 2. For the data presented in this section, the follow-on injections for the multi-injection strategies were close coupled to the initial injection, with the 2nd injection of the 2xDI and 3xDI strategies run at a SOI timing of -240 dATDCf, and the third injection of the 3xDI strategy run at a timing of -210 dATDCf. Retarding spark timing leads to increased exhaust gas temperature as the combustion phasing is retarded towards the exhaust valve opening event. Exhaust gas temperatures of over 800 °C were achieved with both injection strategies at the most retarded timing of 25 dATDCf. The retarded combustion phasing also reduced gross thermal efficiency leading to increased fuel (and air) flow requirements to maintain the desired 2 bar NIMEP load. Almost 3.5x higher fuel flow was required at 25 dATDCf vs at -10 dATDCf to achieve the same engine load. This increase in exhaust flow rate coupled with the increased exhaust gas temperature substantially increased the exhaust heat rate ejected from the cylinder that is subsequently available for catalyst warmup. Similar exhaust temperature and exhaust heat rate trends were observed for both single and double injection strategies. Engine stability was tracked by the coefficient of variation (COV) of NIMEP expressed as a percentage where a higher COV implies lower engine stability. Spark retard in general increased COV for both injection strategies, but operation with 2xDI produced substantial stability gains at all spark timings where it could be employed. Approximately 80% reduction in COV at 10 dATDCf and 40% reduction at 25 dATDCf was observed when switching from the 1xDI to 2xDI strategy.

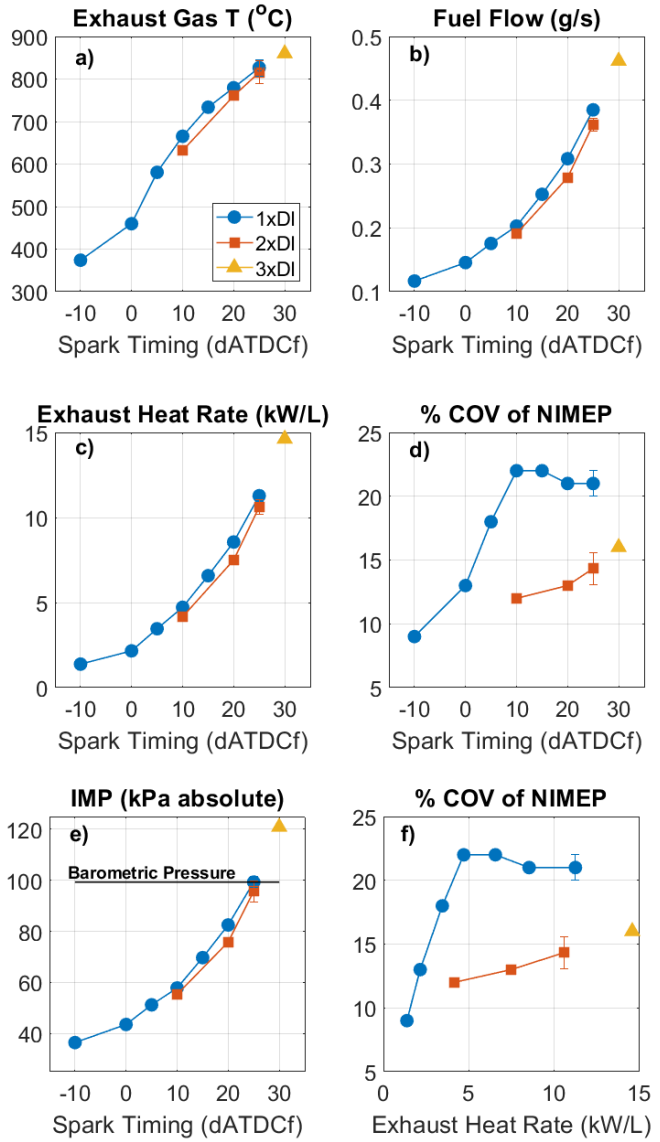

Figure 2: Performance data over spark sweep during cold-start steady-state stoichiometric operation at 2 bar NIMEP with single as well as a double- and triple-split direct injection. Results indicate similar trends in exhaust heat rate across the three strategies, but significant engine stability improvements with the split injection strategies.

The improved COV with 2xDI is consistent with the calculated combustion metrics for the two injection strategies as shown in Figure 3, wherein employing 2xDI not only results in shorter ignition delay (Figure 3a) but also faster flame propagation as evidenced by the shorter time-duration required to achieve 50% mass fraction burned for the same spark timing (Figure 3b). The overall earlier and faster combustion with 2xDI is also illustrated in the apparent heat release rate (AHRR) traces of both 1xDI and 2xDI strategies at the same spark timing of 10 dATDCf (Figure 3c). Similar trends in AHRR were observed to also persist at later timings but are not shown here for brevity. This improvement in 2xDI combustion performance is likely due to the 2xDI strategy creating a more favorable charge-air mixture either through better fuel-air premixing or through stratifications with rich regions near the spark plug. As discussed in the introduction section, Li et al [18] demonstrated through optical measurements that in a close-coupled split injection strategy (as is employed in the current study) the second injection interfaces with the air entrained by the first injection jet which ultimately promotes evaporation of the second injection jet. However, it is not possible to conclusively define the mechanism through which 2xDI improves performance in this study without further optical engine experiments or CFD studies with similar boundary conditions and combustion geometry as is employed in this study.

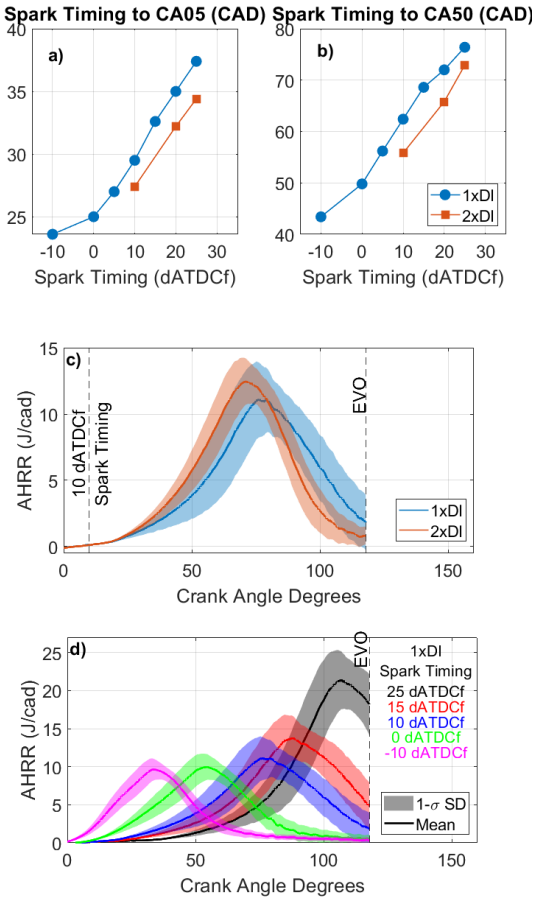

Figure 3: Combustion metrics over spark sweep during cold-start steady-state stoichiometric operation at 2 bar NIMEP with single (1xDI) and double-split (2xDI) direction injection. a) Ignition delay defined as crank angles between spark timing and 5% fuel mass burned (CA05), b) crank angles between spark timing and 50% fuel mass burned, c) apparent heat release rate (AHRR) at spark timing of 10 dATDCf, d) Heat release rate calculated till exhaust valve opening (EVO) timing (118 dATDCf) for spark sweep with 1xDI strategy. For c) and d), solid lines represent mean of 5000 cycles, and shaded regions represent 1-σ standard deviation.

It should be noted that heat release calculations are only performed while the exhaust valve is closed. However, for the very retarded spark timings the heat release was observed to progress beyond EVO timing as illustrated in Figure 3d, and the combustion metrics calculations could be skewed in such cases. Additionally, the significant increase in fuel flow at later spark timings (Figure 2b) also leads to substantial increase in the peak heat release rate (Figure 3d). Finally, the stability advantage of 2xDI not only provides noise, vibration, and harshness (NVH) benefits, but also unlocks substantial gains in exhaust heat rate when the engine is to be operated under a stability constrained regime as is expected at these conditions. When the engine is constrained to a COV < 20%, as prescribed in the ACECTT protocol, operation with 2xDI achieves ~2.5X higher exhaust heat rate as compared to using a single injection.

Generally, engine stability is expected to decrease with spark retard as the ignition is pushed into a lower temperature and lower turbulence regime, which is less favorable for kernel expansion and transition into a propagating flame. This trend is observed for a spark retard of up to 10 dATDCf in the single injection strategy. However, for later spark timings, the COV was observed to plateau even when the spark was retarded to 25 dATDCf. This could be attributed to a combination of three factors; (1) progressive transition of the flame propagation from turbulent to laminar regime as the spark timing is retarded, (2) the significant increase in the combustion charge mass required to meet load at such late spark timings and (3) the deceleration of the piston later in the exhaust stroke thereby constraining the available expansion volume. Ravindran et al [27], showed with CFD simulations that at early spark timing (-10 dATDCf) the flame propagation is predominantly in the corrugated and wrinkled regime, while at very late spark timings (26 dATDCf) the flame propagation transitions from corrugated to laminar regimes. Additionally, as the piston moves towards bottom dead center, the cylinder pressure and total kinetic energy in the cylinder are reduced both of which aid in flame propagation in the laminar regime.

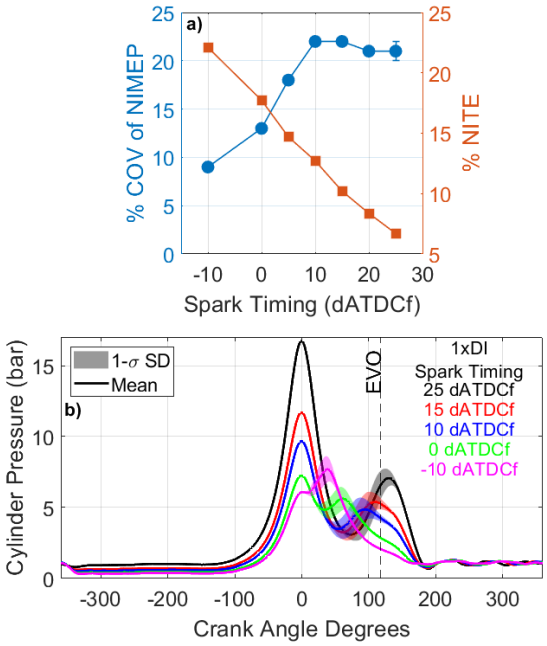

Figure 4: Engine performance metrics over spark sweep during cold-start steady-state stoichiometric operation at 2 bar NIMEP with single (1xDI) direction injection strategy. a) % COV of NIMEP and % NITE, b) Cylinder pressure traces over spark sweep during cold-start steady-state operation at 2bar NIMEP with single direct injection. Solid lines represent mean pressure of 5000 cycles, and shaded regions represent 1-σ standard deviation.

Figure 4 shows the in-cylinder pressure traces (median traces in solid lines as well as shaded 1σ standard deviations) along with the % net thermal efficiency (NTE) for the single injection strategy. During the initial spark retard, the combustion pressure reduces as the ignition and flame propagation are pushed further into the expansion stroke. This is accompanied by the expected increase in engine COV. However, retarding beyond the spark timing of 10 dATDCf led to a reversal of this trend and the combustion pressure started increasing with spark retard due to the increased fueling rate as well as a reduction in the available expansion volume. This increase in combustion pressure is also accompanied by the plateauing of the observed engine COV. Additionally, the % net indicated thermal efficiency (NITE) at very retarded timings is less than 10% indicating that very little of the injected fuel is required to be burned to achieve desired engine load. Finally, the late combustion phasing and associated increase in exhaust gas temperature also increased end-gas and trapped mass temperature which further aids in improving ignition stability and flame propagation.

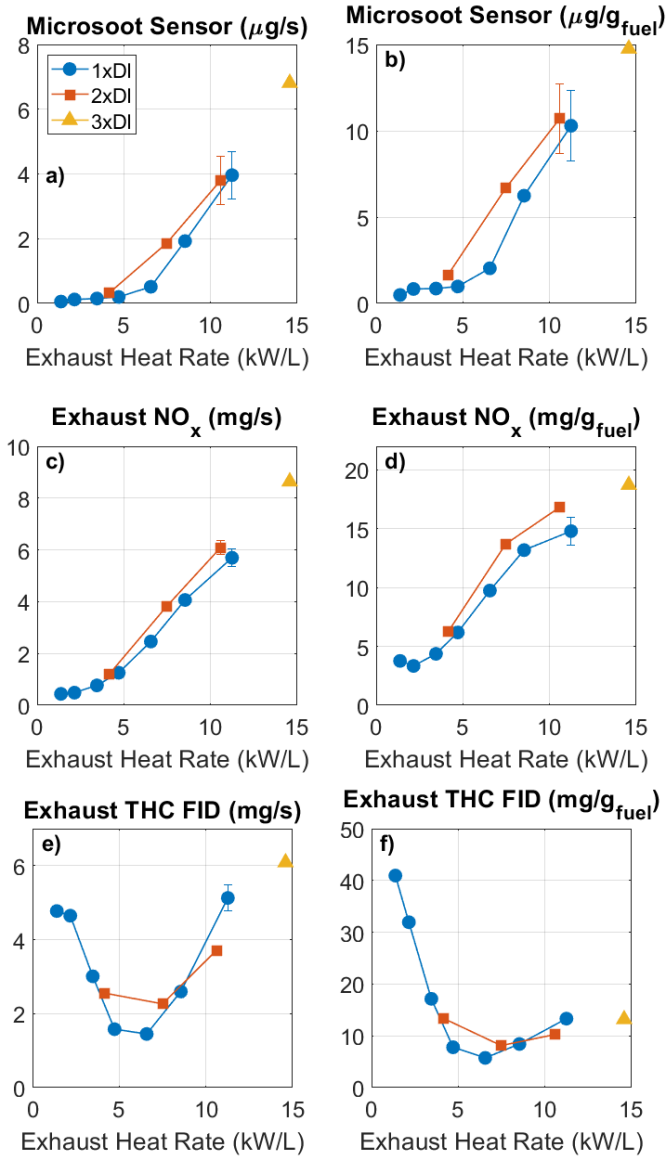

Figure 5: Emissions data over spark sweep during cold-start steady-state stoichiometric operation at 2 bar NIMEP with single as well as a double- and triple-split direction injection. Results show higher soot and NOx emissions with the split injection strategies as compared to the baseline single injection strategy, while similar exhaust hydrocarbons were observed for all three strategies.

Figure 5 shows the emissions measurements as a function of the exhaust heat rate measured across the spark timing sweep in both absolute mass-flowrate and fuel-flow-normalized units. While the absolute mass-flowrate of emissions are more relevant for assessing the impact of various engine control methodologies on catalyst warmup, the fuel-flow-normalized emissions help elucidate differences in the in-cylinder combustion process by correcting for the effect of increased exhaust mass flow on the emissions mass flow. Soot and NOx increase monotonically with spark retard for all injection strategies. The THC emission mass flowrate initially exhibited a sharp decrease with spark retard (Figure 5e) due to higher residual gas temperature as well as continued post exhaust oxidation with THC emissions at spark timing of 15 dATDCf observed to be 70% lower than emissions at -10 dATDCf. However, spark retard beyond 15 dATDCf resulted in an equally strong increase in THC emissions and the THC mass flowrate at 25 dATDCf spark timing was similar to the flowrate at -10 dATDCf timing. When analyzed in fuel-flow-normalized terms (Figure 5f), the initial decrease in THC emissions was much stronger with THC emissions at spark timing of 15 dATDCf observed to be ~86% lower than emissions at -10 dATDCf, while the subsequent increase was much smaller resulting in the emissions at 25 dATDCf still being ~68% lower than the fuel-normalized emissions at -10 dATDCf.. Therefore, the sharp rise in THC mass flowrate at the most retarded spark timings, was primarily due to the substantial increase in the exhaust mas flow rate. The weak rise observed in the fuel-normalized THC is likely due to continued oxidation beyond the sampling location in the exhaust manifold.

Results also indicate slightly higher (~7% @ 25 dATDCf spark timing) NOx emissions with 2xDI strategy as compared to single injection operation. This could be explained by the earlier combustion phasing and shorter burn durations with the 2xDI strategy (Figure 3c) leading to higher in-cylinder temperatures and therefore increased NOx production. Additionally, if 2xDI increases in-cylinder air-fuel-ratio (AFR) stratification, the resultant fuel-lean regions could also contribute to higher NOx emissions. This effect is even stronger when normalized by fuel flow (Figure 5d), wherein the 2xDI strategy produced ~13% higher NOx emissions than 1xDI per unit of fuel burned indicating that the observed increase in NOx emissions is primarily driven by in-cylinder combustion differences between the two strategies. As shown in Figure 5e&f, all injection strategies produced similar THC trends indicating that the global-stoichiometric ratio coupled with long burn durations led to consistent HC oxidation regardless of injection strategy. 2xDI strategy could likely create higher soot emissions (Figure 5a) due to the increased charge stratification. However, the differences in soot emissions between the two strategies are not statistically significant in this study.

The single 3xDI case showed further engine stability and exhaust heat rate improvements while exhibiting similarly higher soot and NOx emissions as the 2xDI case. However, this was a singular point and is only included to demonstrate the potential of higher split injection strategies. A more extensive study with new injection hardware that allows for higher pressures and shorter injection durations would be required to establish trends beyond the 2xDI strategy. Additionally, as previously mentioned, the 3xDI strategy running at 30 dATDCf required boosted operation (26.7 kPa gauge IMP) to achieve the desired 2 bar NIMEP load which may be difficult to achieve in a real engine equipped with turbomachinery.

The fraction of injected fuel lost to engine oil was tracked across the spark timing sweep using the λ_{ratio} and $Fuel_{Loss}$ parameters as defined by Eq 2 and Eq 3.

$$\lambda_{ratio} = \frac{\lambda_{mass}}{\lambda_{emissions}} \quad \text{Eq. 1}$$

$$Fuel_{Loss} = (1 - \lambda_{ratio}) * 100 \quad \text{Eq. 2}$$

where, λ_{mass} is the air-fuel equivalence ratio calculated using air and fuel mass flows, and $\lambda_{emissions}$ is the air-fuel equivalence ratio calculated from emissions measurements. If no fuel is lost to engine oil, then λ_{ratio} would be 1 and $Fuel_{Loss}$ would be 0%. However, if fuel is being lost to engine oil, then the additional fuel required to compensate for this fuel loss will cause λ_{mass} calculation to imply an air-fuel mixture rich in fuel, i.e., lower than 1, while $\lambda_{emissions}$ would still be controlled to stochiometric, i.e., at 1. Therefore, λ_{ratio} would be < 1 and $Fuel_{Loss}$ would be > 0%.

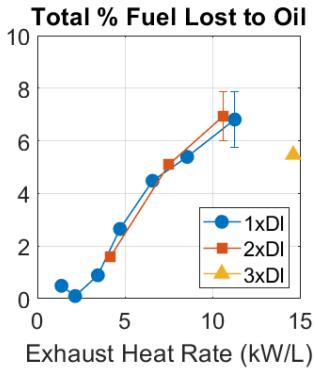

Figure 6: Total % Fuel-loss-to-oil during cold-start operation at various spark timings and single as well as double- and triple-split injection strategies. Results indicate similar fuel-loss behavior with single and double-split strategies while the triple-split strategy could provide potential fuel-loss improvements.

As shown in Figure 6, retarding spark timing led to an increase in the amount of fuel being lost to oil for both 1xDI and 2xDI strategies. These trends are not only consistent with previously reported trends of 1xDI up to 10 dATDC timing [6] and but also continue along the same trajectory for the more retarded spark timings included in this study. Furthermore, when analyzed in exhaust heat rate space both 1xDI and 2xDI strategies produce similar fuel-loss-to-oil trends. This is an unexpected behavior, as the split injection in theory should help in reducing spray penetration, but it is possible that the close-coupled injection profiles employed in this study does not have a significant enough impact on spray penetration and/or atomization to change wall wetting and fuel-loss-to-oil behavior. However, the fuel-loss-to-oil observed with the 3xDI case was ~36% (5.5% vs 9%) lower than the behavior of the 1xDI and 2xDI strategies extrapolated out to 15 kW/L exhaust heat rate. Therefore, higher split strategies could potentially be beneficial in reducing oil-dilution with fuel but require further investigation.

The trends in engine performance parameters (such as COV, fuel-loss-to-oil and exhaust heat rate) as well as engine emissions parameters (such as soot, NOx, and THC) observed with a single injection strategy are consistent with previous results [6] on this engine. In those results, the spark retard was limited to 10 dATDCf timing and the engine was fueled using a market representative gasoline fuel (RD5-87). As a point of comparison, the previous study investigated cold-start operation during a sweep of the exhaust valve opening (EVO) timing where an exhaust heat rate of ~8 kW/L was achieved at an EVO retard of 50 degrees and a spark timing of 10 dATDCf. However, in that case engine stability was severely impacted, showing a COV of 35%. This condition has similar combustion phasing as the 25 dATDCf spark timing zero-EVO retard condition investigated in the current study, and therefore is a good point of comparison. The previous results showed ~60% worse engine stability and ~30% lower exhaust heat rate. Nevertheless, because of the increased valve overlap (due to EVO retard) and the associated increase in trapped mass as well as exhaust rebreathing, HC and NOx emissions were significantly reduced by factors of ~7x and ~4x, respectively, when compared on a per-gram-of-injected-fuel basis. Further, EVO retard provided exhaust heat rate increases without impacting fuel-loss-to-oil behavior for a given spark timing of 10 dATDCf, while the approach of retarding the spark timing applied here led to a ~2.5x increase in the fuel lost to oil and therefore higher oil dilution. This demonstrates a delicate interplay between various engine parameters that could be exploited to maximize exhaust heat rate while minimizing engine out emissions before catalyst light-off.

2xDI - Effect of second injection SOI

The start-of-injection (SOI) spacing between the two direct injections was swept from the initial value of 30 CAD to 70 CAD in three steps at a spark timing of 25 dATDCf, and the engine performance and emissions parameters are illustrated in Figure 7 and Figure 8, respectively. All points were run at the same 2 bar NIMEP stoichiometric condition with the first injection SOI timing of -270 dATDCf. It should be noted that while the baseline point (-240 dATDCf second injection SOI) was run 3 times to establish statistics, the other two points were only run once. Therefore, the single error bars in Figure 7 show the variability observed in the baseline case and are assumed to also be applicable for the other cases. Retarding the SOI of the second injection had negligible impact on engine performance parameters such as COV and exhaust heat rate until an SOI of -210 dATDCf. However, retarding the second injection SOI beyond -210 dATDCf led to a significant degradation of engine stability as evidenced by the 40% increase in COV observed at -200 dATDCf SOI. The in-cylinder charge motion decreases as the SOI is retarded due to reducing piston speed while the time available for mixing is also reduced. This leads to worse air-fuel mixing and therefore worse combustion performance. This hypothesis is further supported by a slight increase of ~25% (~20% increase when normalized by fuel flow) in soot emissions (Figure 8a) observed at -200 dATDCf when compared to earlier SOI timings, indicating the presence of significant AFR gradients.

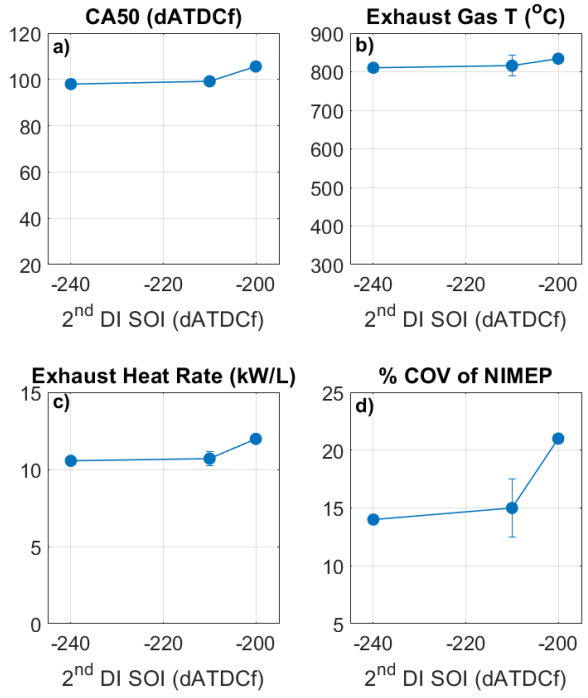

Figure 7: Engine performance data at various SOI timings of the second injection during cold-start operation at 25 dATDCf spark timing and the 2xDI strategy. Results indicate weak trends when 2nd injection SOI is retarded from -240 to -210 dATDCf while engine stability is significantly degraded when SOI is further retarded to -200 dATDCf.

Fuel-flow-normalized NOx emissions (Figure 8d) increased by ~13% when retarding the SOI timing from -240 to -210 dATDCf, but further retardation to -200 dATDCf led to ~10% decrease. This behavior could point to evolving in-cylinder stratification as the second injection SOI is retarded. Generally, the presence of AFR gradients is expected to increase NOx emissions and this was observed when retarding from -240 to -210 dATDCf. However, it is possible that retarding the second injection beyond -210 dATDCf leads to poor enough mixing performance that the resultant AFR gradients are sufficiently lean to suppress NOx production. Fuel-flow-normalized THC emissions (Figure 8f) also exhibited similar trends as NOx emissions wherein retarding the second injection SOI from -240 to -210 dATDCf increased THC emissions by ~17% while further retardation to -200 dATDCf led to a ~28% decrease.

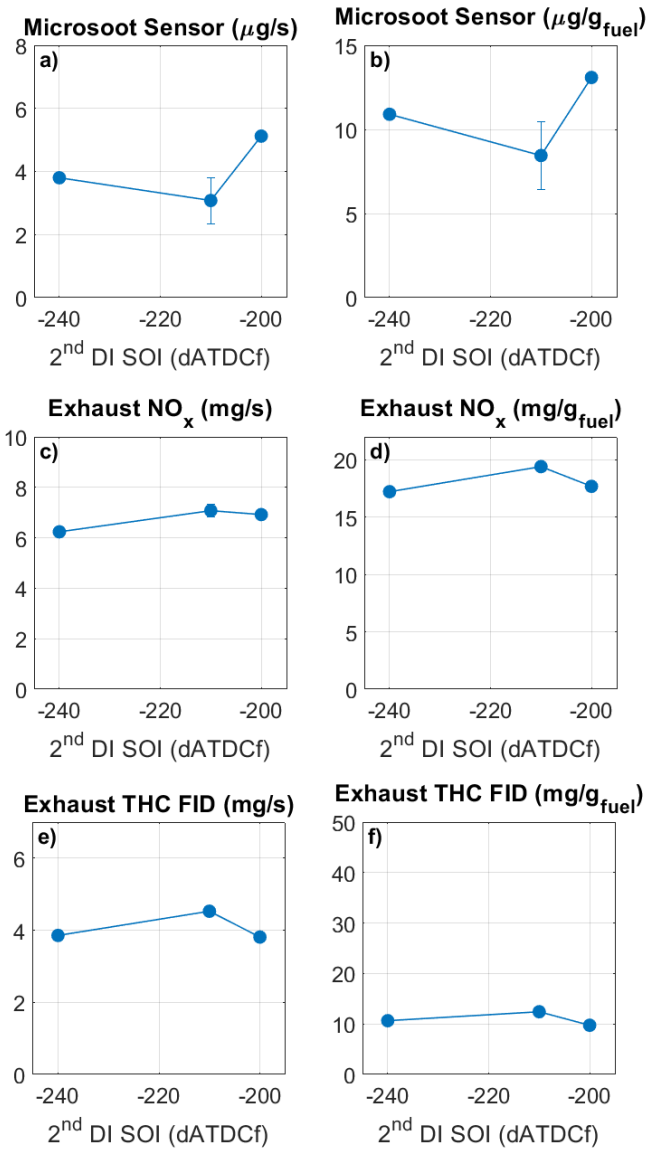

Figure 8: Engine emissions data at various SOI timings of the second injection during cold-start operation at 25 dATDCf spark timing and the 2xDI strategy. Results indicate weak trends in emissions over the second injection SOI sweep range investigated in this study.

This behavior could be an interplay between changing AFR gradients wherein richer regions are likely to increase THC emissions, while the increased exhaust temperature at very retarded second injection SOI would promote late cycle oxidation of the crevice-region THC. Furthermore, the long burn durations coupled with the stoichiometric presence of oxygen in the global mixture also aids in the eventual oxidation of HC trapped in rich and crevice regions as the exhaust gas homogenizes and oxidizes throughout the exhaust stroke and even into the exhaust manifold. Figure 3d illustrated that fuel combustion was continuing even after the exhaust valve opens and the oxidation persisting into the exhaust manifold at this very late combustion phasing is supported by previously reported data [6] wherein the exhaust gas temperature was shown to increase in the exhaust manifold at very late combustion phasing values.

Finally, the fuel-loss-to oil trend was not statistically significant across the second injection SOI sweep. This indicates that the spray and wall-wetting characteristics do not change significantly across the SOI sweep range studied, or the sensitivity of this approach is not sufficient to discriminate changes in wall-wetting with small changes in SOI timing. While the current dataset provides important insights into the impact of second injection timing on cold-start performance and emissions, further experimental testing, in-cylinder spray imaging and/or CFD simulations are required to ascertain how the SOI sweep of second injection impacts mixing in this specific combustion geometry. Additionally, the impact of retarding the second injection into the compression stroke or even into the expansion stroke (just before the spark timing) also needs investigation.

Conclusions

In this study, engine performance, emissions, and catalyst warmup potential were monitored while the engine was operated using a single direct injection (baseline case) as well as a two-way-equal-split direct injection strategy. The two injection strategies were analyzed at a range of cold-start-operation relevant retarded spark timings of up to 25 dATDCf. A stoichiometric 2 bar NIMEP steady-state condition was used for all cases to simulate cold-start operation.

Results indicate that engine stability is negatively impacted when the engine is operated at these late spark timings for faster catalyst warmup. However, multi-injection strategies have the potential to provide significant engine stability improvements allowing for increased exhaust heat rate and therefore faster catalyst warmup. Additionally, this improvement in catalyst warmup with split injection strategies could also help mitigate the increased engine out NOx and (possibly) soot emissions observed with split injection strategies by helping achieve faster catalyst light-off. The improved engine stability with split injection strategies will also have NVH benefits. Both single and two-way-split injection strategies produced similar fuel-loss-to-oil behavior, while the three-way-split point indicated potential fuel-loss-to-oil benefits with higher split injection count. Delaying the second injection timing of the two-way split strategy closer to the bottom dead center negatively impacted engine stability while having minimal impact on emissions.

The data presented in this study would be beneficial as a calibration and validation set for CFD simulations. However, additional experiments – both metal and optical, as well as CFD simulations are required to provide more clarity on the mechanisms driving the trends presented in this study. Furthermore, the qualitative trends observed here are expected to be applicable to different combustion chamber geometries and fuel injection hardware, but the quantitative behavior will likely be hardware dependent.

Acknowledgments

This research was conducted as part of the Partnership to Advance Combustion Engines (PACE) Consortium sponsored by the U.S. Department of Energy (DOE) Vehicle Technologies Office (VTO).

The PACE Consortium is a collaborative project of multiple National Laboratories that combines unique experiments with world-class DOE computing and machine learning expertise to speed discovery of knowledge, improve engine design tools, and enable market-competitive powertrain solutions with potential for best-in-class lifecycle emissions. A special thanks to DOE VTO program managers Mike Weismiller and Gurpreet Singh.

Authors also acknowledge the US Drive ACEC Tech Team, and well as Ronald Grover and Sharon Li from General Motors (USA) for their valuable suggestions and discussions.

References

[1] Chen, Hai-Ying, and Chang Hsiao-Lan (Russell). “Development of Low Temperature Three-Way Catalysts for Future Fuel Efficient Vehicles.” Johnson Matthey Technology Review 59(1), (2015): 64-67. doi:10.1595/205651315X686011.

[2] Myung, Cha-Lee, Kim Juwon, Jang Wonwook, et al. “Nanoparticle Filtration Characteristics of Advanced Metal Foam Media for a Spark Ignition Direct Injection Engine in Steady Engine Operating Conditions and Vehicle Test Modes.” Energies 8(3), (2015): 1865-81. doi:10.3390/en8031865.

[3] Chambon, P., Deter, D., Irick, D. and Smith, D., "PHEV Cold Start Emissions Management," SAE Int. J. Alt. Power. 2(2):2013, doi:10.4271/2013-01-0358..

[4] Qi Liu, Jingping Liu, Jianqin Fu et. al. "Comparative study on combustion and thermodynamics performance of gasoline direct injection (GDI) engine under cold start and warm-up NEDC," Energy Conversion and Management 181, (2019): 663-673. https://doi.org/10.1016/j.enconman.2018.12.043.

[5] McNenl M, Miles PC, Som S, and Szybist JP. "Partnership for Advanced Combustion Engines (PACE) - A Light-Duty National Laboratory Combustion Consortium, " United States: N. p., 2020. Web. https://www.energy.gov/node/4448704

[6] Jatana GS, Chuahy FDF, Szybist JP. "The effect of spark-plug heat dispersal range and exhaust valve opening timing on cold-start emissions and cycle-to-cycle variability.", SAE Int. J. Adv. & Curr. Prac. in Mobility. 2022, 4(2):462-471, https://doi.org/10.4271/2021-01-1180.

[7] Rodriguez, J. and Cheng, W., "Cycle-by-cycle analysis of cold crank-start in a GDI engine," SAE Int. J. Engines 9(2):2016, doi:10.4271/2016-01-0824.

[8] Fedor, W., Kazour, J., Haller, J., Dauer, K. et al., "GDi Cold Start Emission Reduction with Heated Fuel," SAE Technical Paper 2016-01-0825, 2016, doi:10.4271/2016-01-0825.

[9] Rodriguez, J. and Cheng, W., "Reduction of Cold-Start Emissions through Valve Timing in a GDI Engine," SAE Int. J. Engines 9(2):2016, doi:10.4271/2016-01-0827.

[10] Badshah, H., Kittelson, D., and Northrop, W., "Particle Emissions from Light-Duty Vehicles during Cold-Cold Start," SAE Int. J. Engines 9(3):2016, doi:10.4271/2016-01-0997.

[11] Rodriguez, J. and Cheng, W., "Analysis of NOx Emissions during Crank-Start and Cold Fast-Idle in a GDI Engine," SAE Int. J. Engines 10(2):2017, doi:10.4271/2017-01-0796.

[12] Hu, J., Hall, M., Matthews, R., Moilanen, P. et al., “A Novel Technique for Measuring Cycle-Resolved Cold Start Emissions Applied to a Gasoline Turbocharged Direct Injection Engine,” SAE Int. J. Advances & Curr. Prac. in Mobility 2(5):2469-2478, 2020, doi:10.4271/2020-01-0312..

[13] Jaworski, A., Mądziel, M., Kuszewski, H., Lejda, K. et al., “Analysis of Cold Start Emission from Light Duty Vehicles Fueled with Gasoline and LPG for Selected Ambient Temperatures,” SAE Technical Paper 2020-01-2207, 2020, doi:10.4271/2020-01-2207.

[14] Etikyala, S. and Dahlander, P., “Soot Sources in Warm-Up Conditions in a GDI Engine,” SAE Technical Paper 2021-01-0622, 2021, doi:10.4271/2021-01-0622.

[15] Abdulfatah Abdu Yusuf, Freddie L. Inambao. "Effect of cold start emissions from gasoline-fueled engines of light-duty vehicles at low and high ambient temperatures: Recent trends," Case Studies in Thermal Engineering 14, (2019). https://doi.org/10.1016/j.csite.2019.100417.

[16] Longfei Chen, Zhirong Liang, Xin Zhang, Shijin Shuai. "Characterizing particulate matter emissions from GDI and PFI vehicles under transient and cold start conditions," Fuel 189, (2017): 131-140. https://doi.org/10.1016/j.fuel.2016.10.055.

[17] Li, T., Hiroyasu, H., Zhang, Y., and Nishida, K., "Characterization of Mixture Formation Processes in DI Gasoline Engine Sprays with Split Injection Strategy via Laser Absorption and Scattering (LAS) Technique," SAE Technical Paper 2003-01-3161, 2003, https://doi.org/10.4271/2003-01-3161.

[18] Li, T., Nishida, K., Zhang, Y., Yamakawa, M. et al., "An Insight Into Effect of Split Injection on Mixture Formation and Combustion of DI Gasoline Engines," SAE Technical Paper 2004-01-1949, 2004, https://doi.org/10.4271/2004-01-1949.

[19] Mittal M, Hung DLS, Zhu G, Schock HJ. Fuel spray visualization and its impingement analysis on in-cylinder surfaces in a direct-injection spark-ignition engine. J Visualization 2011;14(2):149–60. https://doi.org/10.1007/s12650-011-0083-0

[20] Cedrone, K. and Cheng, W., "SI Engine Control in the Cold-Fast-Idle Period for Low HC Emissions and Fast Catalyst Light Off," SAE Int. J. Engines 7(2):968-976, 2014, https://doi.org/10.4271/2014-01-1366.

[21] Reiche, D., Wooldridge, S., Moilanen, P., and Davis, G., "Experimental Optimization of the Cold Start for the EcoBoost Engine," SAE Technical Paper 2009-01-1491, 2009, https://doi.org/10.4271/2009-01-1491.

[22] Yi, J., Wooldridge, S., Coulson, G., Hilditch, J. et al., "Development and Optimization of the Ford 3.5L V6 EcoBoost Combustion System," SAE Int. J. Engines 2(1):1388-1407, 2009, https://doi.org/10.4271/2009-01-1494.

[23] Stiesch, G., Merker, G., Tan, Z., and Reitz, R., "Modeling the Effect of Split Injections on DISI Engine Performance," SAE Technical Paper 2001-01-0965, 2001, https://doi.org/10.4271/2001-01-0965.

[24] Zheng Z, Tian X, Zhang X. Effects of split injection proportion and the second injection time on the mixture formation in a GDI

engine under catalyst heating mode using stratified charge strategy. Appl Therm Eng 2015;84:237–45. https://doi.org/10.1016/j.applthermaleng.2015.03.041.

[25] Kim, Sung-Jun and Hyun, Soungjae and Park, JaeIn, "Optimization of Cold Start Operating Conditions in a Stoichiometric GDI Engine with Wall-guided Piston using CFD Analysis," SAE Technical Paper 2013-01-2650. (2013) https://doi.org/10.4271/2013-01-2650.

[26] Asami, S. and Shiraishi, T., "Availability of Balanced Truncation for Reducing an Automotive Cold Start Engine Model," SAE Int. J. Engines 9(2):2016, doi:10.4271/2016-01-9152.

[27] Ravindran AC, Kokjohn SL, Petersen B. "Improving computational fluid dynamics modeling of Direct Injection Spark Ignition cold-start". International Journal of Engine Research. 2021;22(9):2786-2802. doi:10.1177/1468087420963982.

[28] Edwards K.D. 2022. "Simulation of Spray, Wall-Film, and Charge Preparation for Light-Duty, Cold-Start Applications." ASME 2022 Internal Combustion Engines Forward Conference, ICEF 2022 V001T06A010.

[29] S. W. Wagnon, 2021. "Development of an Optimized Gasoline Surrogate Formulation for PACE Experiments and Simulations." Advanced Engine and Fuel Technologies Program 2020 Annual Progress Report, U.S. Department of Energy Vehicles Technology Office, https://www.energy.gov/sites/default/files/2021-07/VTO_2020_APR_ADV_FUEL_COMPILED_REPORT_JUL_7_2021_compliant_.pdf

[30] https://www.energy.gov/sites/default/files/2018/03/f49/ACEC_TT_Roadmap_2018.pdf

[31] Dempsey A, Ghandhi J. "Engine Emissions & Uncertainty Analysis," [Online].; 2015 [cited 2015 12 29]. Available from: http://sourceforge.net/projects/engine-emissions-uncertainty/files/.

Contact Information

Gurneesh S. Jatana
National Transportation Research Center
Oak Ridge National Laboratory
2360 Cherahala Boulevard
Knoxville, TN 37932
jatanags@ornl.gov

Definitions/Abbreviations

ATDCf	After Top Dead Center Firing
BTDC	before top dead center
CA50	crank angle @ 50% fuel burn
CAD	Crank Angle Degrees
COV	coefficient of variation
DISI	Direct Injected Spark Ignited
ECS	engine control system
EVO	Exhaust Valve Opening
GDI	gasoline direct injection
HR	Spark Plug Heat Range
IMP	Intake Manifold Pressure
LHV	Lower Heating Value
MBT	Minimum spark advance for maximum brake torque
NIMEP	Net Mean Effective Pressure
NITE	Net Indicated Thermal Efficiency
NVH	Noise, Vibration, and Harshness
ORNL	Oak Ridge National Laboratory
SI	spark ignition
TDCf	Top Dead Center firing
THC	Total Hydrocarbons